# Cellulose Nanocrystals and Au Nanoparticles Well-Dispersed in a Poly(styrene-b-ethylene oxide) Block Copolymer Matrix

**ARTICLE** *in* THE JOURNAL OF PHYSICAL CHEMISTRY C · OCTOBER 2011

Impact Factor: 4.77 · DOI: 10.1021/jp2054958



**4 AUTHORS**, INCLUDING:

Agnieszka Tercjak
Universidad del País Vasco / Euskal Herriko …
**119** PUBLICATIONS **1,175** CITATIONS
SEE PROFILE

Gurutz Mondragon
Universidad del País Vasco / Euskal Herriko …
**10** PUBLICATIONS **21** CITATIONS
SEE PROFILE

THE JOURNAL OF PHYSICAL CHEMISTRY C

ARTICLE

pubs.acs.org/JPCC

# Cellulose Nanocrystals and Au Nanoparticles Well-Dispersed in a Poly(styrene-*b*-ethylene oxide) Block Copolymer Matrix

Agnieszka Tercjak,* Junkal Gutierrez, Gurutz Mondragon, and Iñaki Mondragon*

Materials + Technologies Group, Dpto. Ingeniería Química y M. Ambiente, Escuela Politécnica, Universidad País Vasco/Euskal Herriko Unibertsitatea, Pza. Europa 1, 20018 Donostia-San Sebastián, Spain

**ABSTRACT:** Cellulose nanocrystals (CNCs) were used to prepare novel polymeric composites based on a self-assembled poly(styrene-*b*-ethylene oxide) (PS-*b*-PEO) block copolymer with and without Au nanoparticles synthesized using $HAuCl_4$ as a precursor. Taking into account the hydrophilic behavior of the CNCs, well-dispersed cellulose nanocrystals were confined in the PEO block due to hydrogen-bond interactions. Electrical properties of pristine CNC cellulose nanocrystals and their PS-*b*-PEO based composites with and without conductive Au nanoparticles were studied using electrostatic force microscopy. Results indicate that CNC cellulose nanocrystals respond to the voltage applied to the EFM tip independent of the sign of the applied voltage. Addition of conductive Au nanoparticles into the CNC/PS-*b*-PEO composite led to the highest contrast between charged and uncharged domains. Designed materials responded to the increasing or decreasing voltage cycles almost without hysteresis even on the macroscale, as measured by a semiconductor analyzer.

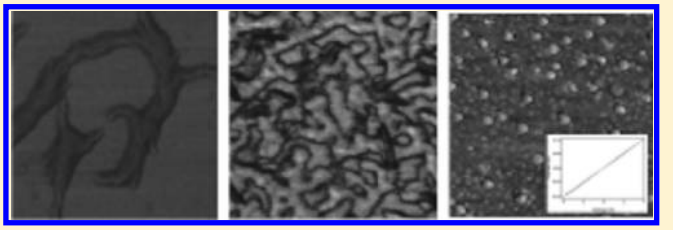

## INTRODUCTION

Nowadays, block copolymers are an interesting class of materials, which can be used as templates for inorganic fillers.[1−14] Block copolymers can be self-assembled to form nanoscale structures with a domain spacing that depends on molecular weight, segment size, and the strength of the interaction between the blocks. In selective solvents, diblock copolymers are able to form micelles of various morphologies, such as spheres, cylinders, vesicles, etc. In the bulk, microphase separation occurs, leading to various microstructures, such as spheres, hexagonally packed cylinders, lamellae, and discontinuous phases.[1,6] The ability to control both the length scale and the spatial organization of block copolymer morphologies makes these polymeric materials particularly attractive candidates for use as templates in the preparation of hybrid inorganic/organic materials.

On the other hand, cellulose nanocrystals (CNCs) have been recently investigated as an attractive environmentally friendly nanomaterial for the preparation of low-cost nanocomposites.[15−21] CNCs are highly crystalline, rodlike nanofillers obtained from wood biomass resources by acid hydrolysis.[22−25] One promising application of these cellulose-based nanomaterials is to use them as nanofillers in polymer composites, mainly taking into account their high crystallinity (70−95%), outstanding Young's modulus of 130−150 GPa, and electrical properties.[26,27] However, based on our knowledge, this is the first time when a block copolymer was used as a template in order to confine cellulose nanocrystals in one of the blocks, which can open new fields of applications of these novel composites with interesting electrical properties.

In the present work, novel composites containing cellulose nanocrystals and synthesized Au nanoparticles (generated using a $HAuCl_4$ precursor) well-confined in a self-assembled poly(styrene-*b*-ethylene oxide) (PS-*b*-PEO) diblock copolymer matrix were designed. Cellulose nanocrystals acted as a directing agent for confinement of Au nanoparticles in PEO-block domains. Electrical properties of investigated materials were studied using electrostatic force microscopy (EFM). Electrical properties of nanofillers located in the PEO block of the PS-*b*-PEO block copolymer proved that designed materials pose interesting specific properties and can open new fields of application in different areas of nanotechnology.

## EXPERIMENTAL SECTION

**Materials.** Amphiphilic poly(styrene-*b*-ethylene oxide) diblock copolymer (PS-*b*-PEO), Polymer Source Inc., was used as a template agent. The number-average molecular weight, $M_n$, for PS (PEO) blocks and the $M_w/M_n$ of block copolymers were 58 600 (31 000) g $mol^{-1}$ and 1.04, respectively. The gold precursor used was gold(III) chloride hydrate ($HAuCl_4$, pure ∼46% as Au), purchased from Sigma-Aldrich and used as received. Chloroform (trichloromethane) supplied by Sigma-Aldrich was used as a solvent and used as received.

Cellulose nanocrystals were extracted from Avicel microfillers (Sigma-Aldrich), following sulfuric acid hydrolysis and centrifugation processes, as published in the literature.[22−25] The resulting white solid product was centrifuged at 9000 rpm at room temperature for 15 min and washed with distilled water. The centrifugation/washing cycles were repeated 10 times. Finally,

**Received:** June 12, 2011
**Revised:** August 25, 2011
**Published:** October 05, 2011





dx.doi.org/10.1021/jp2054958 | *J. Phys. Chem. C* 2011, 115, 22180–22185

cellulose nanowhiskers were freeze-dried and ground into powder.

**Blending Protocol.** The designed CNC/PS-*b*-PEO and Au-CNC/PS-*b*-PEO composites were prepared following the same procedure. First, CNC cellulose nanocrystals were sonicated in chloroform at room temperature by using a microprocessor sonicator 750 W (Vibracell 75043 from Bioblock Scientific) with an amplitude range between 20 and 25%. After 1 h, the required amount of PS-*b*-PEO block copolymer and/or $HAuCl_4$ as Au nanoparticles precursor were added. These mixtures were again sonicated for an additional 30 min at the same conditions. Finally, CNC/PS-*b*-PEO and Au-CNC/PS-*b*-PEO systems were cast on Si(100) wafers by using a Telstar Instrumat P-6708D spin-coater (2000 rpm, 60 s).

Here, it should be pointed out that all prepared composites contain 1 wt % of nanofillers with different ratios between Au nanoparticles and CNCs (50:50, 25:75, 75:25).

**Morphological Analysis.** Atomic force microscopy (AFM) images were obtained operating in tapping mode with a scanning probe microscope (Nanoscope IIIa, Multimode$^{TM}$ from Digital Instruments, Veeco) equipped with an integrated silicon tip/cantilever having a resonance frequency of ~300 kHz, from the same manufacturer. To obtain repeatable results, different regions of the specimens were scanned. Similar images were obtained, thus demonstrating the reproducibility of the results.

Electrostatic force microscopy was used to confirm electrical properties of both CNC cellulose nanocrystals and synthesized Au nanoparticles. Measurements were performed using a scanning probe microscope (Nanoscope IVa, Dimension 3100 from Digital Instruments) operating in the Lift-Mode (lift height was around 200 nm) in ambient conditions and equipped with an integrated Co/Cr-coated MESP tip having a resonance frequency around 75 kHz. The secondary imaging mode derived from the tapping mode that measures electric field gradient distribution above the sample surface was detected by applying a voltage to the cantilever tip. Locally charged CNC cellulose nanocrystals and synthesized Au nanoparticles were qualitatively mapped.

**Differential Scanning Calorimetry.** DSC measurements were carried out in a Mettler Toledo DSC 822 differential scanning calorimeter equipped with a Sample Robot TSO 801 RO. Nitrogen was used as a purge gas (10 mL/min). Measurements were performed in sealed aluminum pans containing a sample weight of approximately 5 mg. The temperature was calibrated by using an indium standard. To ensure comparable thermal history, all samples were first heated to 150 °C and maintained at that temperature for 10 min, then cooled to −25 °C and reheated to 150 °C. All the scans were performed at a constant rate of 5 °C $min^{-1}$.

A semiconductor characterization system (Keithley model 4200-SCS) was used to study the conductive properties of the materials. Two-point probe experiments were carried out applying current from −4 to 4 V and from 4 to −4 V to verify the response of the investigated systems.

## ■ RESULTS AND DISCUSSION

Figure 1a shows a representative AFM phase image of cellulose nanocrystals, which were isolated form Avicel cellulose by acid hydrolysis and suspended in chloroform using a ultrasonicator. As can be clearly observed, CNCs showed a rodlike shape with 15−20 nm in diameter and 250−400 nm in length.

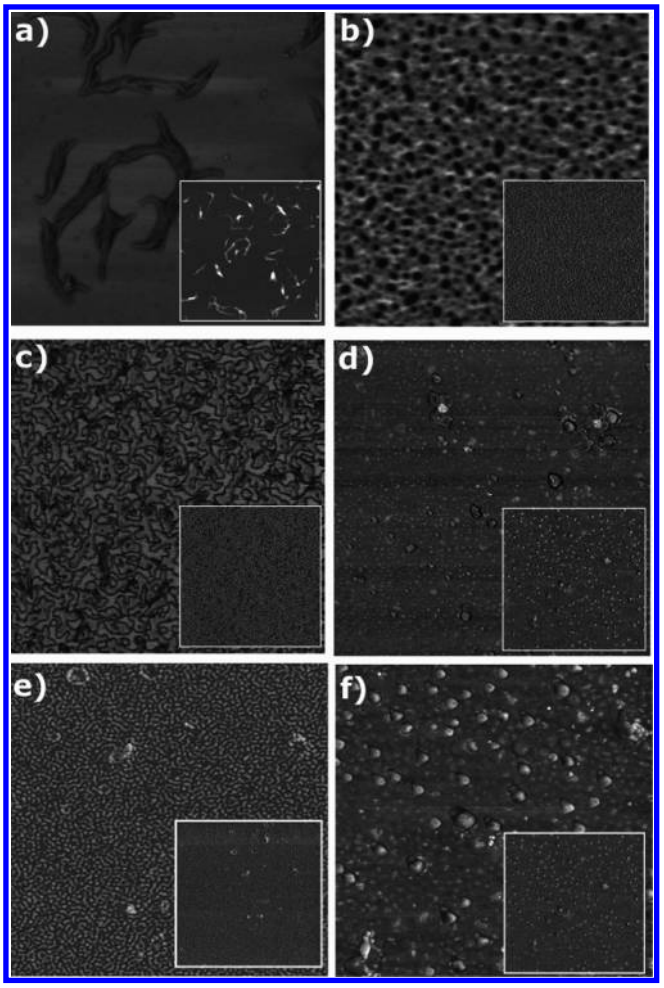


**Figure 1.** AFM phase images (3 $\mu$m × 3 $\mu$m) of (a) CNC cellulose nanocrystals; (b) PS-*b*-PEO block copolymer; and (c) 1 wt % CNC/PS-*b*-PEO, (d) 1 wt % Au-CNC(50:50)/PS-*b*-PEO, (e) 1 wt % Au-CNC-(25:75)/PS-*b*-PEO, and (f) 1 wt % Au-CNC(75:25)/PS-*b*-PEO composites. The insets correspond to 15 $\mu$m × 15 $\mu$m AFM images.

Under preparation conditions, some of the cellulose nanocrystals were aggregated in the image. However, one can easily distinguish individual cellulose nanocrystals spin-coated on the silica wafer.

A representative AFM phase image of the PS-*b*-PEO diblock copolymer is shown in Figure 1b. Taking into account that the modulus of PS is higher than that for PEO, the darker microphase-separated zones correspond to PEO-block domains and the brightest zones correspond to PS-block domains.[10,28,29] Under preparation conditions, using chloroform as a solvent, the self-assembled PS-*b*-PEO block copolymer showed a wormlike morphology, with a size distribution of the microphase-separated PS-block domains of 40−65 nm in diameter.

A typical AFM phase image of 1 wt % CNC/PS-*b*-PEO composites is shown in Figure 1c. Under the same preparation conditions, the introduction of 1 wt % CNC into the PS-*b*-PEO block copolymer changed the morphology to gyroid-like from wormlike micelles corresponding to a neat self-assembled PS-*b*-PEO block copolymer. The changes in the morphology and good dispersion of cellulose nanocrystals in the PS-*b*-PEO block matrix can be related to hydrogen-bond interactions between −OH groups of CNC and PEO-block chains.[18] Moreover, well-dispersed CNC cellulose nanocrystals appeared confined in the

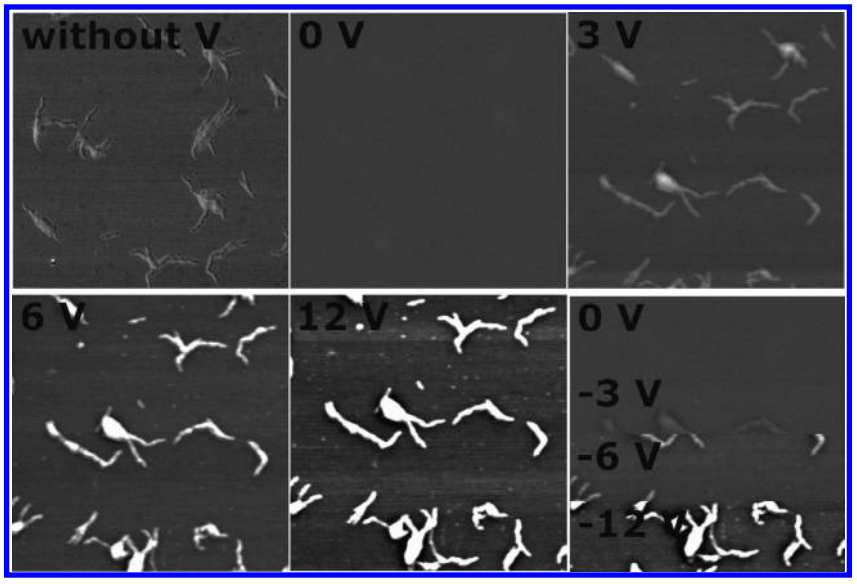


**Figure 2.** EFM phase images (5 $\mu$m × 5 $\mu$m) of CNC cellulose nanocrystals taken without (the gray color scale = 18°) and with Lift Mode (the gray color scale = 2°) applying 0, 3, 6, 12, −3, −6, and −12 V.

microphase-separated PEO-block phase. Thus, cellulose nanocrystals separated within the PEO block of block copolymers provoked that PEO-block domains appeared bigger and denser in the phase image. Here, it should be pointed out that no aggregation of cellulose nanocrystals was detected, as clearly shown in the inset of Figure 1c.

As shown in Figure 1d, the morphology of the designed composites changed significantly when 0.5 wt % Au nanoparticles and 0.5 wt % CNC cellulose nanocrystals were added to the PS-*b*-PEO block copolymer. The AFM phase image indicated good confinement of the synthesized Au nanoparticles with an average size of 80−110 nm in diameter. Taking into account the size of synthesized Au nanoparticles, it becomes difficult to distinguish the microphase-separated PEO block. However, as published by Mendoza et al.[34,35] and by us,[14] PEO-block-rich domains appeared as brighter zones, thus indicating that synthesized Au nanoparticles can interact with the PEO block of the block copolymer. Here, it should be pointed out that, in this case, strong hydrogen-bond interactions can take place between the Au nanoparticle precursor and cellulose nanocrystals.[20,21] Consequently, even not well-distinguished (indicated with arrows in Figure 1d) cellulose nanocrystals were located with synthesized Au nanoparticles in the PEO block of the PS-*b*-PEO block copolymer. Addition of 1 wt % Au-CNC with the ratio of 25:75 (Figure 1e) led to the system with very well established microphase separation of the blocks of PS-*b*-PEO. Under the same preparation conditions, similar to 1 wt % CNC/PS-*b*-PEO composites, the final morphology of this composite was different if we compare with the morphology of the neat PS-*b*-PEO block copolymer. This fact confirmed the good dispersion of the cellulose nanocrystals, which are confined in the PEO block of the used block copolymer.[18] Thus, well-dispersed cellulose nanocrystals changed the ratio between the PS block and CNC/PEO-block-rich phase, consequently leading to a different morphology. Simultaneously, as expected, a lower amount of synthesized Au nanoparticles in 1 wt % Au-CNC(25:75)/PS-*b*-PEO if compared to 1 wt % Au-CNC(25:75)/PS-*b*-PEO was detected. On the contrary, as shown in Figure 1f, addition of 1 wt % Au-CNC with the ratio of 75:25 into the PS-*b*-PEO block copolymer did not allow detection of the microphase separation of the PS-*b*-PEO block copolymer due to generation of 80−120 nm in diameter, well-dispersed synthesized Au nanoparticles. AFM phase images (Figure 1d,f) indicated that the morphological behavior of the nanocomposites that contain 1 wt % Au-CNC(75:25) is very similar to the system that contains 1 wt % Au-CNC(50:50).

As it is well known from the literature, both cellulose nanocrystals and Au nanoparticles show electrical properties. Taking this into account, the electrical properties of the investigated materials were investigated using electrostatic force microscopy. In this qualitative method, different positive and negative voltages are applied into the EFM tip, which, consequently, allows one to detect charged domains. Here, it should be pointed out that, as it is well-known,[30−33] the positively charged domains appear dark in the EFM phase image and the negatively charged domains appear bright. Representative EFM images of cellulose nanocrystals are shown in Figure 2. Here, it should be pointed out that the EFM phase image of the CNC is different if compared to the AFM phase image, which is due to the different both resolution and coating of the tip used for EFM measurement. The EFM image of CNCs clearly showed that no charged domains were detected on the surface of the investigated systems if 0 V was applied to the EFM tip. On the contrary, applying 3 V into the EFM tip allowed us to distinguish charged domains, which corresponded to cellulose nanocrystals. Moreover, an increase of the positive voltage applied to the EFM tip (6 and 12 V) led to higher contrast between charged and uncharged areas of the samples, especially taking into account that the contrast level of all EFM phase images (0, 3, 6, and 12 V) was around 2°. As it is shown in the bottom-right image of Figure 2 (EFM images applying negative voltage, −3, −6, and −12 V), the increase of the negative voltage led to the appearance of charged areas with higher contrast, which clearly corresponded to cellulose nanocrystals. Consequently, cellulose nanocrystals responded in the whole range of the voltage applied into the EFM tip, regardless of the sign of the applied voltage.

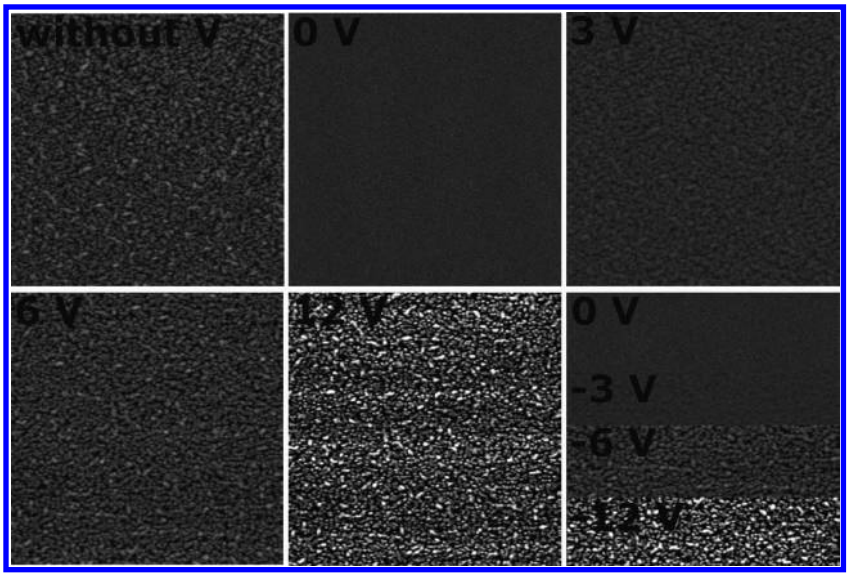


**Figure 3.** EFM phase images (5 $\mu$m × 5 $\mu$m) of the 1 wt % CNC/PS-*b*-PEO composite taken without (the gray color scale = 18°) and with Lift Mode (the gray color scale = 2°) applying 0, 3, 6, 12, −3, −6, and −12 V.

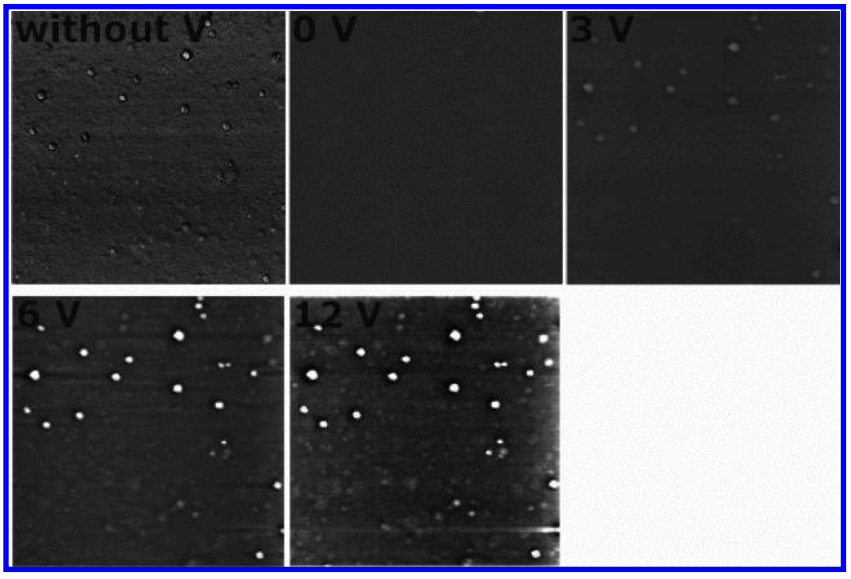


**Figure 4.** EFM phase images (5 $\mu$m × 5 $\mu$m) of 1 wt % Au-CNC/PS-*b*-PEO taken without (the gray color scale = 18°) and with Lift Mode (the gray color scale = 2°) applying 0, 3, 6, and 12 V.

EFM phase images of 1 wt % CNC/PS-*b*-PEO applying different voltages into the EFM tip are shown in Figure 3. As for EFM images taken for pristine cellulose nanocrystals, to ensure that the measurement was performed without the influence of the topography of the sample, first, 0 V was applied to the EFM tip. When 0 V was applied to the EFM tip, no charged domains were detected on the surface of the investigated composite (see 0 V EFM image). This fact confirmed that the topography of this sample did not have any influence on the performed measurements. Applying 3, 6, and 12 V to the EFM tip allowed us to clearly distinguish two microphase-separated phases, and only one of them responded to the applied voltage. Here, it should be pointed out that, although not shown, the PS-*b*-PEO block copolymer did not respond to the voltage applied to the EFM tip. Taking both results into account, one can conclude that well-dispersed CNC cellulose nanocrystals were located in PEO-block domains of the block copolymer. As in the case of pristine cellulose nanocrystals, the increase of voltage led to higher contrast between charged and uncharged domains. The same behavior was observed when negative voltage was applied to the EFM tip, indicating that cellulose nanocrystals retained their electrical properties in the designed composite.

The typical EFM images of the 1 wt % Au-CNC/PS-*b*-PEO composite taken applying different positive voltages to the EFM tip are shown in Figure 4. Under the same EFM measurement conditions, the designed composite showed similar, but higher contrast, behavior than that for both CNC cellulose nanocrystals and the 1 wt % CNC/PS-*b*-PEO composite. Applying 0 V to the EFM tip proved that no charged areas were detected on the surface of this sample. On the contrary, applying 3, 6, and 12 V to

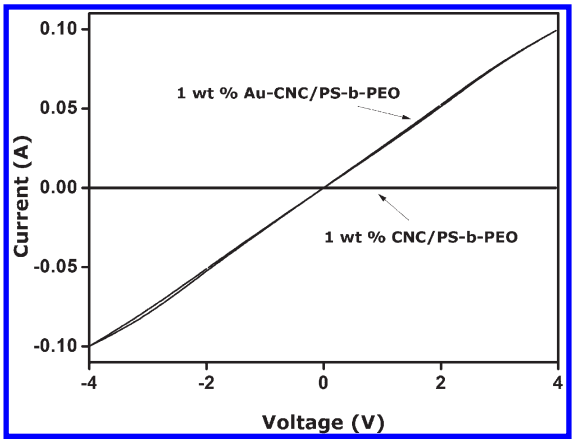


**Figure 5.** Voltage−current curves of pristine CNCs, 1 wt % CNC/PS-*b*-PEO, and 1 wt % Au-CNC/PS-*b*-PEO by Keithley.

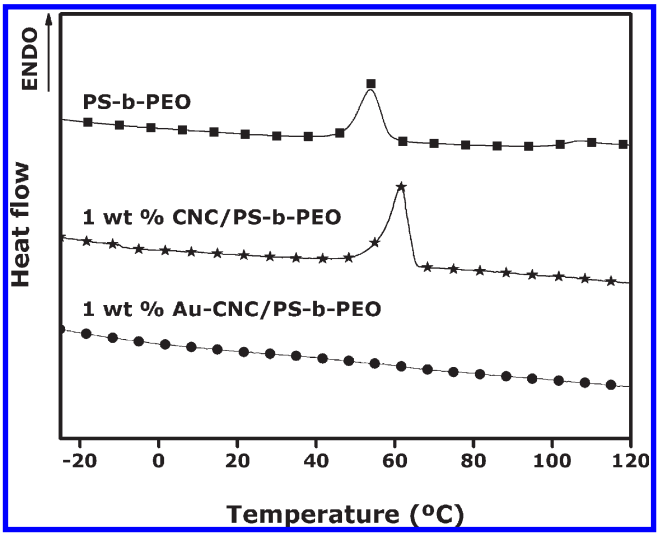


**Figure 6.** DSC thermograms of the neat PS-*b*-PEO block copolymer and 1 wt % CNC/PS-*b*-PEO and 1 wt % Au-CNC/PS-*b*-PEO composites.

the EFM tip allowed us to detect charged domains. Comparing the EFM image without voltage and EFM images taken applying voltage to the EFM tip, one can easily conclude that the charged domains corresponded to the synthesized Au nanoparticles and CNCs. Moreover, the contrast between charged and uncharged domains increased with increasing the voltage applied to the EFM tip. Although not shown here, the negative voltage applied to the EFM tip led to higher contrast between charged and uncharged domains.

The current−voltage ($I-V$) curves of 1 wt % CNC/PS-*b*-PEO and 1 wt % Au-CNC/PS-*b*-PEO composites were obtained by means of a semiconductor analyzer. Two-point probe experiments were carried out, applying voltage from −4 to 4 V and from 4 to −4 V to record the response of the investigated materials (Figure 5). Here, it should be pointed out that pristine CNCs cannot be measured using this method due to lack of the continuity in the sample. Under the same measurement conditions, the 1 wt % CNC/PS-*b*-PEO composite does not respond on the macroscopic scale by applying the voltage cycle using a semiconductor analyzer. On the contrary, the 1 wt % Au-CNC/PS-*b*-PEO composite responded to the increasing or decreasing voltage cycles almost without hysteresis (see Figure 5). It seems that the good distribution of the conductive inorganic nanofiller allowed the current to pass throughout the investigated composites. Therefore, the conductivity presented by the composite containing both Au nanoparticles and CNCs can be related to the fact that synthesized Au nanoparticles show higher conductivity than cellulose nanocrystals. Indeed, the PS-*b*-PEO block copolymer acted as a template for synthesized Au nanoparticles and CNCs, allowing one to design materials with high electrical properties. Moreover, here, it should be once more pointed out that both CNCs and Au nanoparticles retained their electrical properties at nanoscale responding to the voltage applied to the EFM tip.

DSC thermograms of neat PS-*b*-PEO block copolymers and 1 wt % CNC/PS-*b*-PEO and 1 wt % Au-CNC/PS-*b*-PEO composites are shown in Figure 6. As expected, the melting point of the PEO block of the block copolymer appeared at 53 °C. Addition of cellulose nanocrystals shifted the melting temperature of the PEO block to higher temperature, 61 °C. This result indicated the strong influence of cellulose nanocrystals on the melting behavior of the PEO block, once more confirming that cellulose nanocrystals interacted with the PEO block. Moreover, the enthalpy of the melting process of the PEO block in the PS-*b*-PEO block copolymer was lower than the enthalpy of the PEO block in 1 wt % CNC/PS-*b*-PEO composites, being 3.2 and 4.78 J $g^{-1}$, respectively. This phenomenon can be related to the fact that cellulose nanocrystals can act as a nucleating agent for the crystallization of the PEO block, thus increasing the melting enthalpy.[20,21,36−38] On the other hand, under the same measurement condition, the melting point of the PEO block in the 1 wt % Au-CNC/PS-*b*-PEO composite was not detected, indicating that generated Au nanoparticles hindered the crystallization of the PEO block in the block copolymer.

## CONCLUSIONS

Cellulose nanocrystals (CNCs) and composites based on a self-assembled poly(styrene-*b*-ethylene oxide) diblock copolymer (PS-*b*-PEO) modified with cellulose nanocrystals without and with synthesized Au nanoparticles were prepared and characterized. As was clearly distinguished in AFM phase images, CNCs appeared confined in the PEO block of the microphase-separated PS-*b*-PEO block copolymer. Electrostatic force microscopy was employed in order to qualitatively study the electrical behavior at the nanoscale of cellulose nanocrystals and in situ synthesized Au nanoparticles. Both CNCs and synthesized Au nanoparticles retained their conductive properties in the designed CNC/PS-*b*-PEO and Au-CNC/PS-*b*-PEO composites responding to the voltage applied to the EFM tip in the whole positive and negative ranges. Moreover, the good dispersion of Au nanoparticles and their regular size in the Au-CNC/PS-*b*-PEO inorganic/organic composite led to materials that also responded at the macroscale to increasing or decreasing voltage cycles applied using a semiconductor analyzer.

## AUTHOR INFORMATION

### Corresponding Author

*E-mail: agnieszka.tercjaks@ehu.es (A.T.), inaki.mondragon@ehu.es (I.M.).

## ■ ACKNOWLEDGMENT

Financial support from the Basque Country Government in the frame of ETORTEK iNANOGUNE (IE09-243), Grupos Consolidados (IT-365-07), and SAIOTEK2010 (NANOTES, S-PE10UN40) is gratefully acknowledged. The authors wish to also thank the Spanish Ministry of Science and Innovation for the project MAT-2009-06331. Additionally, J.G. thanks Eusko Jaurlaritza/Gobierno Vasco (Programas de becas para formación y perfeccionamiento de personal investigador), and A.T. acknowledges MICINN for the Ramón y Cajal program (RYC-2010-05592). Moreover, we are grateful to the Macrobehavior-Mesostructure-Nanotechnology SGIker unit of the UPV/EHU.

## ■ REFERENCES

(1) Bockstaller, M. R.; Lapetnikov, Y.; Margel, S.; Thomas, E. L. *J. Am. Chem. Soc.* **2003**, *125*, 5276–5277.
(2) Park, S.; Wang, J.-Y.; Kim, B.; Russell, T. P. *Nano Lett.* **2008**, *8*, 1667–1672.
(3) Park, S.; Kim, B.; Wang, J.-Y.; Russell, T. P. *Adv. Mater.* **2008**, *20*, 681–685.
(4) Zhang, Q.; Gupta, S.; Emrick, T.; Russell, T. P. *J. Am. Chem. Soc.* **2006**, *128*, 3898–3899.
(5) Horiuchi, S.; Fujita, T.; Hayakawa, T.; Nakao, Y. *Langmuir* **2003**, *19*, 2963–2973.
(6) Darling, S. B.; Yufa, N. A.; Cisse, A. L.; Bader, S. D.; Sibener, S. J. *Adv. Mater.* **2005**, *17*, 2446–2450.
(7) Lee, J. I.; Cho, S. H.; Park, S.-M.; Kim, J. K.; Kim, J. K.; Yu, J. W.; Kim, Y. Ch.; Russell, T. P. *Nano Lett.* **2008**, *8*, 2315–2320.
(8) Gaines, M. K.; Smith, S. D.; Samseth, J.; Bockstaller, M. R.; Thompson, R. B.; Rasmussen, K. O.; Spontak, R. J. *Soft Matter* **2008**, *4*, 1609–1612.
(9) Garcia, I.; Tercjak, A.; Zafeiropoulos, N.; Stamm, M.; Mondragon, I. *Macromol. Rapid Commun.* **2007**, *28*, 2361–2365.
(10) Gutierrez, J.; Tercjak, A.; Garcia, I.; Peponi, L.; Mondragon, I. *Nanotechnology* **2008**, *19*, 155607.
(11) Garcia, I.; Tercjak, A.; Rueda, L.; Mondragon, I. *Macromolecules* **2008**, *41*, 9295–9398.
(12) Gutierrez, J.; Tercjak, A.; Mondragon, I. *J. Am. Chem. Soc.* **2010**, *132*, 873–878.
(13) Peponi, L.; Tercjak, A.; Luigi, T.; Kenny, J. M.; Mondragon, I. *Compos. Sci. Technol.* **2008**, *68*, 1631–1636.
(14) Tercjak, A.; Gutierrez, J.; Mondragon, I. *J. Phys. Chem. C* **2011**, *115*, 1643–1648.
(15) Yermolenko, I. S.; Lishko, V. K.; Ugarova, T. P.; Magonov, S. N. *Biomacromolecules* **2011**, *12*, 370–379.
(16) de Mesquita, J. P.; Donnici, C. L.; Pereira, F. V. *Biomacromolecules* **2010**, *11*, 473–480.
(17) Holt, B. L.; Stoyanov, S. D.; Pelan, E.; Paunov, V. N. *J. Mater. Chem.* **2010**, *20*, 10058–10070.
(18) Kloser, E.; Gray, D. G. *Langmuir* **2010**, *26*, 113450–13456.
(19) Okita, Y.; Fujisawa, S.; Saito, T.; Isogai, A. *Biomacromolecules* **2011**, *12*, 518–522.
(20) Mahmoud, K. A.; Male, K. B.; Hrapovic, S.; Luong, J. H. *ACS Appl. Mater. Interfaces* **2009**, *1*, 1383–1386.
(21) Shin, Y.; Bae, I. T.; Arey, B. W.; Exarhos, G. J. *J. Phys. Chem. C* **2008**, *112*, 4844–4848.
(22) Capadona, J. R.; van den Berg, O.; Capadona, L. A.; Schroeter, M.; Rowan, S. J.; Tyler, D. J.; Weder, C. *Nat. Nanotechnol.* **2007**, *2*, 765–769.
(23) Beecher, J. F. *Nat. Nanotechnol.* **2007**, *2*, 466–467.
(24) Dong, X. M.; Revol, J. F.; Gray, D. G. *Cellulose* **1998**, *5*, 19–32.
(25) Beck-Candanedo, S.; Roman, M.; Gray, D. G. *Biomacromolecules* **2005**, *6*, 1048–1054.
(26) Eichhorn, S. J.; Dufresne, A.; Aranguren, M.; Marcovich, N. E.; Capadona, J. R.; Rowan, S. J.; Weder, C.; Thielemans, W.; Roman, M.; Renneckar, S.; Gindl, W.; Veigel, S.; Keckes, J.; Yano, H.; Abe, K.; Nogi, M.; Nakagaito, A. N.; Mangalam, A.; Simonsen, J.; Benight, A. S.; Bismarck, A.; Berglund, L. A.; Peijs, T. *J. Mater. Sci.* **2010**, *45*, 1–33.
(27) Iwamoto, S.; Kai, W.; Iwata, T.; Isogai, A. *Biomacromolecules* **2009**, *10*, 2571–2576.
(28) Gutierrez, J.; Tercjak, A.; Garcia, I.; Mondragon, I. *Nanotechnology* **2009**, *20*, 225603.
(29) Tercjak, A.; Serrano, E.; Garcia, I.; Ocando, C.; Mondragon, I. *Acta Mater.* **2007**, *55*, 6436–6443.
(30) Lu, R.; Wu, S. T.; Xu, K. *J. Appl. Phys.* **2003**, *42*, 1628–1632.
(31) Yan, M.; Bernstein, G. H. *Surf. Interface Anal.* **2007**, *39*, 354–358.
(32) Ng, C. Y.; Chen, T. P.; Lau, H. W.; Liu, Y.; Tse, M. S.; Tan, O. K. *Appl. Phys. Lett.* **2004**, *85*, 2941–2943.
(33) Bechtold, I. H.; Batalioto, F.; Thieghi, L. T.; Honda, B. S. L.; Pojar, M.; Schoenmaker, J.; Santos, A. D.; Zucolotto, V.; Balogh, D. T.; Oliveira, O. N.; Oliveira, E. A. *Phys. Rev. E* **2006**, *74*, 0217141.
(34) Mendoza, C.; Pietsch, T.; Gutmann, J. S.; Jehnichen, D.; Gindy, N.; Fahmi, A. *Macromolecules* **2009**, *42*, 1203–1211.
(35) Mendoza, C.; Gindy, N.; Gutmann, J. S.; Fromsdorf, A.; Forster, S.; Fahmi, A. *Langmuir* **2009**, *25*, 9571–9578.
(36) Siqueira, G.; Bras, J; Dufresne, A. *Polymers* **2010**, *2*, 728–765.
(37) Lu, J.; Wang, T.; Drzal, L. T. *Composites, Part A* **2008**, *39*, 738–746.
(38) Suryanegara, L.; Nakagaito, A. N.; Yano, H. *Compos. Sci. Technol.* **2009**, *69*, 1187–1192.